Progress In Electromagnetics Research C, Vol. 51, 63–70, 2014

Broadband Radial Waveguide Power Combiner with Improved Isolation among Adjacent Output Ports

Alaa A. Sarhan[1, *], Nader Ghadimi[1], Emad Hamidi[1], and Homayoon Oraizi[2]

Abstract—An eight-way waveguide-based power combiner/divider is presented and investigated in the frequency range 7.5–10.5 GHz. A simple approach is proposed for design purposes. The measured combiner shows a good agreement between the simulated and measured results. Insertion loss is about −0.3 dB, return loss is less than −15 dB and isolation between adjacent output ports is better than −11 dB at 8.5 GHz and reaches about −14 dB at 9.5 GHz.

1. INTRODUCTION

High power amplifiers play a critical role in the overall performance of microwave and millimeter-wave transmitter chains of radar and communication systems. Current available RF power levels cannot be achieved by a single solid-state device. Consequently, high-efficiency power combiners are required to generate high powers [1–8].

Tree-combiners, namely series combiners, have the disadvantage of using several couplers and transmission lines, which add losses and degrade the combining efficiency, especially for large numbers of combining ports. On the other hand, parallel combiners do not have such disadvantages due to their short combining paths [9]. Often the waveguide technology is superior in many applications, due to its low loss, high power handling capacity and relatively large operational bandwidth. Radial combiner (RC) structures lead to a wider operating bandwidth with over 90% combining efficiency when their various sections and junctions are carefully designed [10].

In this paper, a wideband 8-way radial divider/combiner is presented in the X-band using a conical feed probe connected to a 50 Ohm SMA connector as a matching system. The peripheral ports are standard WR90 waveguides. Also, metallic vertical irises are placed between adjacent outports inside the radial waveguide to improve the isolation between the peripheral ports.

2. ANALYSIS AND DESIGN

Figure 1 shows the radial waveguide-based 8-way power divider/combiner structure. The peripheral waveguide ports are placed radially. The structure is axially symmetric with respect to the central port. A conical transmission line is used to match the radial waveguide to the 50 Ohm SMA connector. The core of the SMA must be connected perfectly to the upper surface of the conical probe to reduce the insertion loss; also the Teflon insulator of the SMA connector must touch the same probe surface.

The characteristic impedance of conical transmission line shown in Figure 2 is

$$Z_0 = \frac{\eta_0}{2\pi} \ln \left[\frac{\cot\left(\frac{\theta_1}{2}\right)}{\cot\left(\frac{\theta_2}{2}\right)} \right] \tag{1}$$

where $\eta_0 = 120\,\pi\Omega$ is the intrinsic impedance of free space.

Received 28 April 2013, Accepted 9 June 2014, Scheduled 16 June 2014

* Corresponding author: Alaa Aldin Sarhan (alaaaldinn@gmail.com).

[1] Department of Electrical Engineering, Malek Ashtar University of Technology, Tehran 15875-1774, Iran. [2]Department of Electrical Engineering, Iran University of Science and Technology, Narmak, Tehran 16844, Iran.

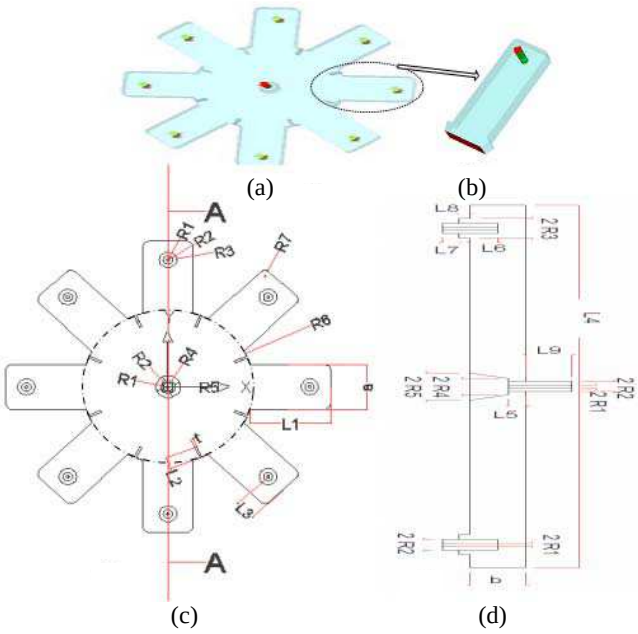

Figure 1. Topology of the RC. (a) 3D view. (b) Output port (adapter with air ring to make it broadband). (c) Top view. (d) Profile at section AA.

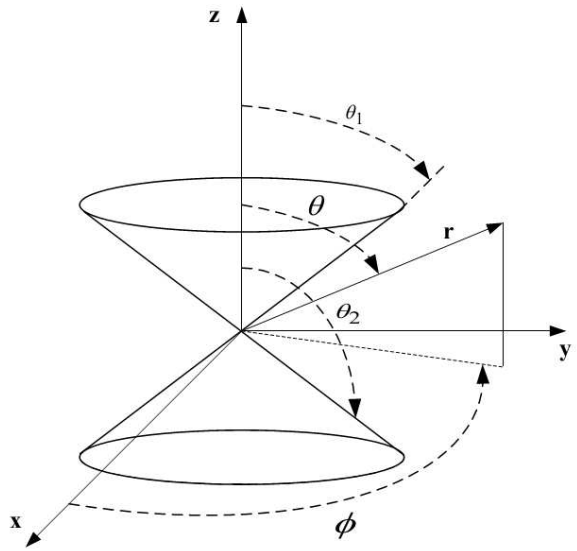

Figure 2. Geometry of a conical transmission line.

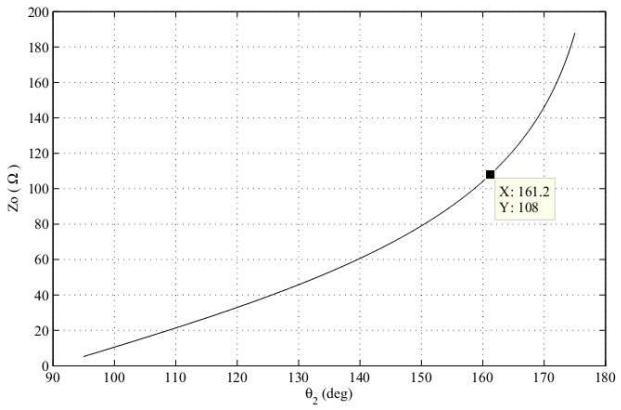

Figure 3. Characteristic impedance of the conical transmission line versus θ_2.

For the design purposes of the proposed structure, $\theta_1 = 90°$, then

$$Z_0 = 60 \ln \left[\tan \left(\frac{\theta_2}{2} \right) \right] \tag{2}$$

Equation (2) shows that the characteristic impedance is not a function of radial distance; it also represents the input impedance of the infinite line at its feed terminals. It is apparent that this transmission line is inherently a very broad-band structure since its characteristic or input impedance is only a function of its geometry (the angle of the cones) and not of frequency. The characteristic

impedance of the conical line is shown in Figure 3 versus its apex angle θ_2.

The radial waveguide operates in the dominant mode for ($h \leq \lambda/2$) where **h** is the height of waveguide, this mode is remarkably simple. As shown in Figure 4, the E-field is merely in the **z** direction, while the H-field lines are concentric circles with respect to the waveguide axis. Both H and E fields vary only in the radial direction **r** and are independent of the z and angular directions. Also, both are orthogonal to radial direction **r**. Consequently, the dominant mode is actually a TEM mode.

In fact, this field configuration is identical to that of a parallel plate waveguide shown in Figure 5, with a characteristic impedance of

$$Z_0 = \frac{\eta}{\sqrt{\varepsilon}_r} \frac{h}{w} \tag{3}$$

where ε_r is the relative dielectric constant of the medium, **h** and **w** are the height and width of the line,

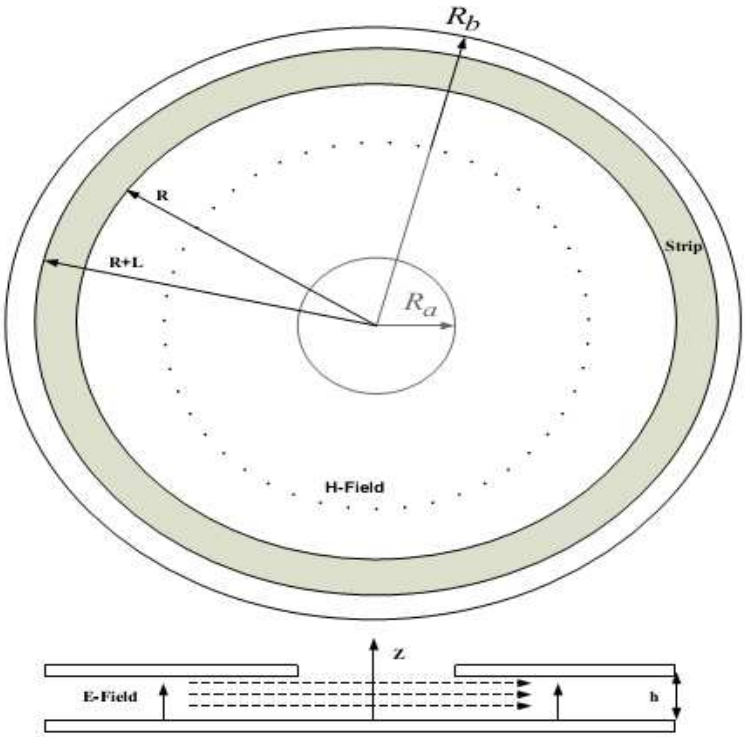

Figure 4. Radial waveguide.

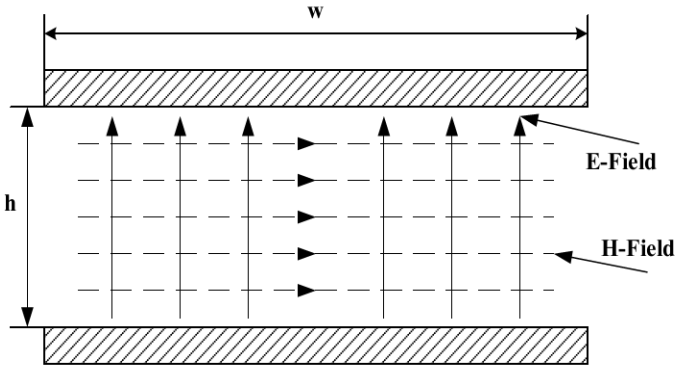

Figure 5. Ideal parallel plate waveguide.

respectively.

Applying Equation (3) to the radial waveguide, its characteristic impedance becomes

$$Z_0 = \frac{\eta}{\sqrt{\varepsilon}_r} \frac{h}{2\pi R} \tag{4}$$

The radial waveguide can be envisaged as many narrow adjacent concentric strips, each strip being a transmission line in the radial direction, for which constant characteristic impedance can be assumed. Then when all the strips are cascaded, they will form a complete radial line. To formulate the problem, a curvature parameter is defined as follows [11]

$$C_r = \frac{2\pi\,(R+L) - 2\pi R}{2\pi R} = \frac{L}{R} \tag{5}$$

To keep this curvature parameter constant, **L** (the width of a strip) must be varied in proportion to its radius. Under this condition, the widths of the strips and their radii follow a geometric progression with a ratio

$$\alpha = 1 + C_r \tag{6}$$

The average radius of the first strip is

$$R_{1avg} = R_a + \frac{L}{2} = R_a \left(1 + \frac{C_r}{2}\right) \tag{7}$$

The progressions of the average radii of subsequent circular strips are

$$R_{1avg}, R_{1avg}\alpha, R_{1avg}\alpha^2, R_{1avg}\alpha^3, \ldots \tag{8}$$

The characteristic impedance of the first strip using Equation (4) is

$$Z_{01} = \frac{\eta}{\sqrt{\varepsilon}_r} \frac{h}{2\pi R_{1avg}} \tag{9}$$

The progression of the characteristic impedances of subsequent strips has a ratio of $1/\alpha$, which is the reverse of that of radii

$$Z_{01}, \frac{Z_{01}}{\alpha}, \frac{Z_{01}}{\alpha^2}, \frac{Z_{01}}{\alpha^3} \cdots \tag{10}$$

Finally, the relationship between the inner and outer radii of the radial waveguide (namely R_a and R_b) is

$$\alpha^n = \frac{R_b}{R_a} \tag{11}$$

where n is the number of circular strips to be determined.

The procedure for calculation of characteristic impedances of the radial lines according to the preceding relations is summarized in the flow chart in Figure 6. The characteristic impedance progression of the radial line versus its average radius progression is shown in Figure 7.

Now a simple algorithm is proposed for design purposes

- By using a full wave 3D simulation software like CST or HFSS design the adapter to cover the desired frequency bandwidth (Figure 1(b)) (in this article the WR90 and the coaxial probe with air ring are chosen).
- Take the definition of modified power-voltage for the waveguide characteristic impedance $Z_0 = \frac{b}{a} Z_{w(\mathrm{TE10})}$ [12] and compute its average on the specified frequency bandwidth, then divide the result by N, the number of the peripheral waveguide ports (in this article $N = 8$).
- Use the curve shown in Figure 7 to determine the outer radius of radial line (R_b).
- Use the curve shown in Figure 3 to determine the characteristic impedance of the conical line (choosing a reasonable value for $R_a = R_5$, in this article $R_a = 5.6\,\mathrm{mm}$ is chosen), then determine R_4 of the cone (see Figures 1(c) and (d)).
- By computer simulation (CST or HFSS) optimize L_5, R_6 and L_2 (see Figures 1(c) and (d)) to obtain the desired reflection and isolation between adjacent peripheral ports (keep in mind that R_6 must stay as minimum as possible to avoid higher order modes).

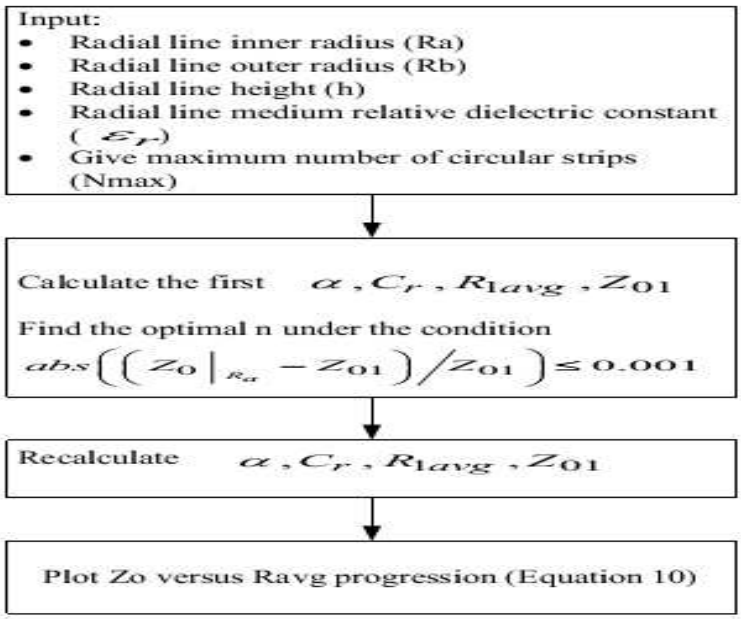

Figure 6. Flow chart used to calculate radial line characteristic impedance at any **r**.

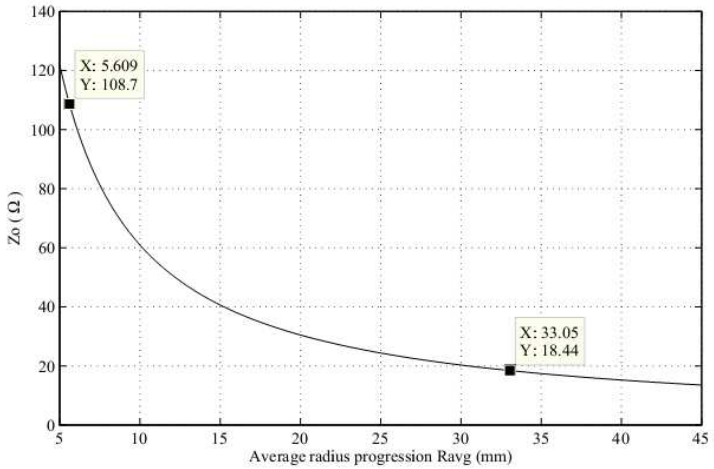

Figure 7. Radial line characteristic impedance versus its average radius progression.

3. SIMULATION AND EXPERIMENTAL RESULTS

Following the simple algorithm proposed before, the adapter shown in Figure 1(b) is simulated and optimized using CST MWS and the result of simulation is shown in Figure 8.

The average characteristic impedance of the waveguide port for this adapter is about 18 Ohm (after dividing by 8 and taking $a = 24.3$ mm for the waveguide port of the adapter). From the curve shown in Figure 7, it is found that $R_6 = 33$ mm. For example, if we select $R_a = R_5 = 5.6$ mm, then the characteristic impedance of the radial line at this radius is about 108 Ohm, this extracted from the curve shown in Figure 7. From the curve shown in Figure 3, if the characteristic impedance of the conical line is taken as 108 Ohm, then $R_4 = 3.3$ mm is obtained. Now by optimizing L_5, R_6 and L_2 the whole design is obtained. The structure dimensions are given in Table 1.

The fabricated combiner is shown in Figure 9 (the material is the brass).

The measurement was done by using the VNA HP8510. The adapters are from Marconi Instruments and the waveguide matching loads are picked from the shelf in the laboratory. Measured and simulated reflection s-parameters are shown in Figure 10.

Observe the good agreement between the simulated and measured results. The measured reflections are all below -15 dB in the frequency range 7.5–10.5 GHz. The little difference between the simulated and measured results is due to the used adapter, which is different from the one used in simulation. The transmission s-parameters are shown in Figure 11. The insertion loss is about -0.3 dB after extracting the adapter loss, which was about -0.2 dB. It is obvious that there is a resonance at 11 GHz. This is because of the cavity resonance.

Figure 12 shows a good linear transmission phases. The phase difference between peripheral

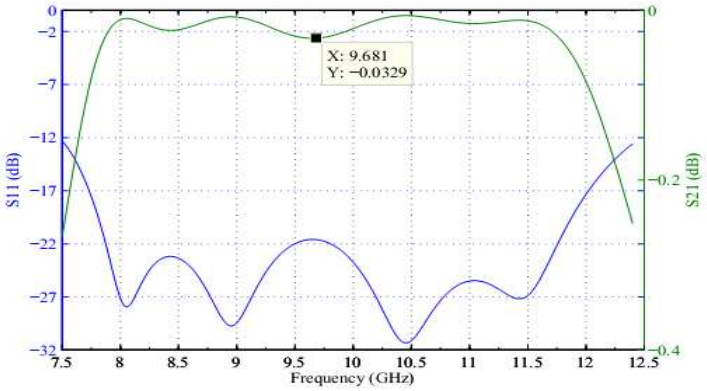

Figure 8. Simulated s-parameters of the adapter.

Table 1. Structure detailed dimensions (mm).

R_1	0.65	a	22.86	L_6	5
R_2	2.1	b	10.16	L_7	3
R_3	4	L_1	36.7	L_8	2
R_4	3.3	L_2	6	L_9	8.4
R_5	5.6	L_3	9.5	t	1
R_6	39	L_4	148		
R_7	3	L_5	3.1		

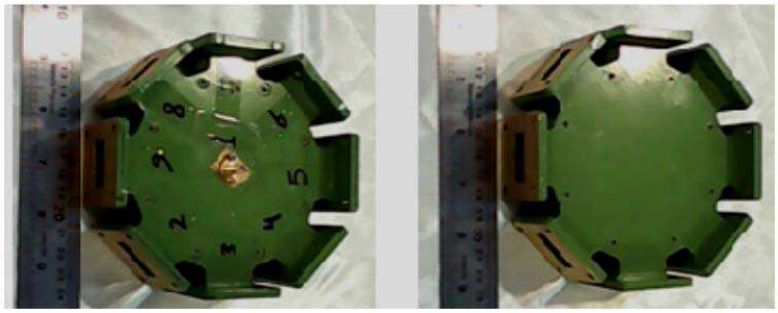

(a) (b)

Figure 9. Fabricated combiner structure without the coaxial-to-waveguide adapter ((a) top view, (b) bottom view).

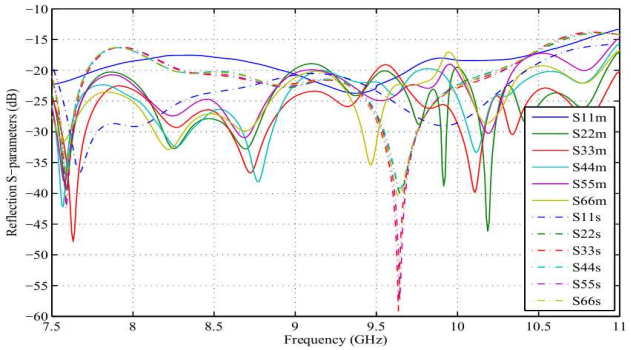

Figure 10. Simulated and measured reflection s-parameters (m index means measured and s index means simulated).

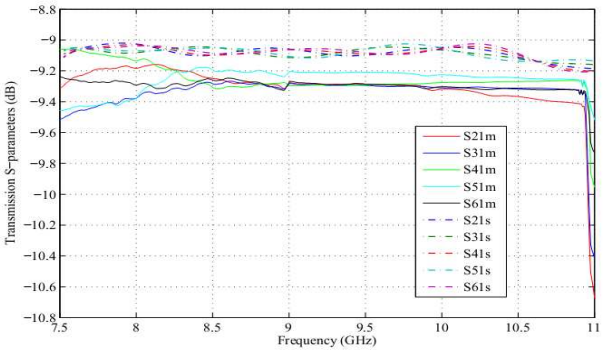

Figure 11. Simulated and measured transmission s-parameters (m index means measured and s index means simulated).

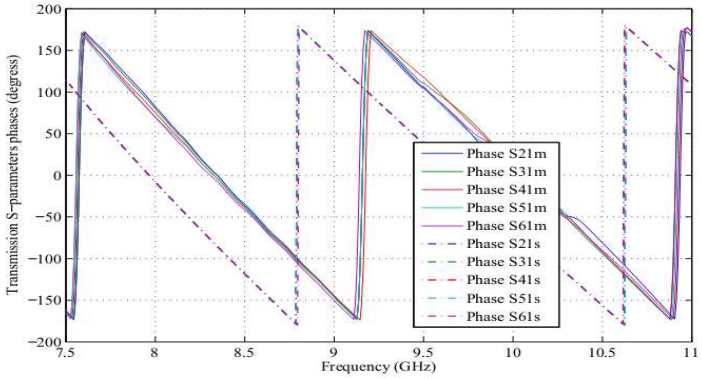

Figure 12. Simulated and measured transmission s-parameters phases (m index means measured and s index means simulated).

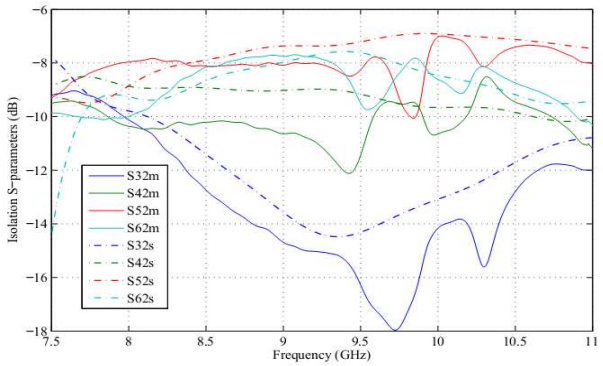

Figure 13. Simulated and measured isolation s-parameters (m index means measured and s index means simulated).

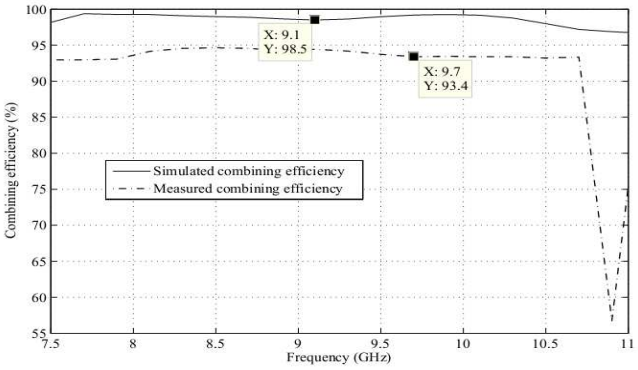

Figure 14. Simulated and measured combining efficiency.

waveguide ports is small and this serves the combining efficiency.

Isolation s-parameters are shown in Figure 13. The coincidence between the measured and simulated results is remarkable. The isolation between adjacent waveguide peripheral ports is better than others because of the used metallic vertical irises inserted symmetrically in the radial line. These vertical irises have a length compatible with the center frequency of the desired frequency bandwidth

in order to make an odd number multiple of the fourth waveguide wavelength $\lambda_g/4$.

The combining efficiency (CE) is calculated by taking the measured and simulated s-parameters into the ADS software, and then Figure 14 is obtained.

It shows a good CE, better than 92% in the frequency range 7.5–10.5 GHz. Also, CE degrades dramatically about the resonance frequency 11 GHz.

4. CONCLUSION

In this paper, a passive waveguide-based power combiner is analyzed and measured using a simple approach. It shows a good agreement between measured and simulated results and an improvement in isolation between adjacent waveguide peripheral ports due to the metallic vertical irises inserted symmetrically in the radial line section. It works in the frequency range 7.5–10.5 GHz and shows a CE better than 92%.

REFERENCES

1. Zhang, Z., D. Zhu, and D. Liu, "A wideband 8-way radial divider/combiner with stepped impedance transformers in Ka band," *2012 IEEE MTT-S International Microwave Workshop Series on Millimeter Wave Wireless Technology and Applications (IMWS)*, 1–4, Nanjing, China, Sep. 18–20, 2012.
2. Dong, Y., S.-W. Dong, and Y. Wang, "A 60 GHz solid-state power combining system," *2012 IEEE MTT-S International Microwave Workshop Series on Millimeter Wave Wireless Technology and Applications (IMWS)*, 1–4, Nanjing, China, Sep. 18–20, 2012.
3. Russell, K., "Microwave power combining techniques," *IEEE Trans. Microwave Theory and Techniques*, Vol. 27, 472–478, 1979.
4. Chang, K. and C. Sun, "Millimeter-wave power-combining techniques," *IEEE Trans. Microwave Theory and Techniques*, Vol. 31, No. 2, 91–107, 1983.
5. Villiers, D. I. L., P. W. Walt, and P. Meyer, "Design of a ten-way conical transmission line power combiner," *IEEE Trans. Microwave Theory and Techniques*, Vol. 55, 302–308, 2007.
6. Song, K., Y. Fan, and Z. He, "Broadband radial waveguide spatial combiner," *IEEE Microwave and Wireless Components Letters*, Vol. 18, 73–75, 2008.
7. Jia, P. C., L. Y. Chen, A. Alexanian, and R. A. York, "Multioctave spatial power combining in oversized coaxial waveguide," *IEEE Trans. Microwave Theory and Techniques*, Vol. 50, 1355–1360, 2002.
8. Cheng, N. S., P. Jia, D. B. Rensch, and R. A. York, "A 120-W X-band spatially combined solid-state amplifier," *IEEE Trans. Microwave Theory and Techniques*, Vol. 47, No. 12, 2557–2561, 1999.
9. Fathy, A. E., S. W. Lee, and D. Kalokitis, "A simplified design approach for radial power combiners," *IEEE Trans. Microwave Theory and Techniques*, Vol. 54, No. 1, 247–255, 2006.
10. Belohoubek, E., R. Brown, H. Johnson, A. Fathy, D. Bechtle, D. Kalokitis, and E. Mykietyn, "30-way radial power combiner for miniature GaAs FET power amplifiers," *1986 IEEE MTT-S International Microwave Symposium Digest*, Vol. 86, 515–518, Jun. 1986.
11. Franco, S. and B. Marina, *Solid-state Microwave High-power Amplifiers,* 1st Edition, Artech House, London, UK, 2009.
12. Tang, W. and X. B. Yang, "Design of Ka-band probe transitions," *IEEE International Conference on Applied Superconductivity and Electromagnetic Devices (ASEMD)*, 25–28, Sydney, NSW, Dec. 11–16, 2011.